Pediatric RESEARCH

BASIC SCIENCE ARTICLE

# Human ucMSCs seeded in a decellularized kidney scaffold attenuate renal fibrosis by reducing epithelial–mesenchymal transition via the TGF-β/Smad signaling pathway

Dong Hu[1,2,3], Deying Zhang[1,2], Bo Liu[1,2], Yang Liu[4], Yu Zhou[1,2], Yihang Yu[1,2], Lianju Shen[2], Chunlan Long[2], Dan Zhang[2], Xing Liu[1,2], Tao Lin[1,2], Dawei He[1,2], Tao Xu[5], Peter Timashev[6], Denis Butnaru[7], Yuanyuan Zhang[8] and Guanghui Wei[1,2]

**BACKGROUND:** Renal fibrosis occurs largely through epithelial–mesenchymal transition (EMT). This study explored the beneficial effects of a human umbilical cord mesenchymal stem cell-loaded decellularized kidney scaffold (ucMSC-DKS) on renal fibrosis in a rodent model of post-transplantation renal failure, and the underlying mechanism.
**METHODS:** Rat-derived DKSs were examined after preparation, and then recellularized with human ucMSCs to prepare cell-loaded patches. A rat model of renal failure was established after subtotal nephrectomy (STN). The cell patches were transplanted to remnant kidneys. Changes in renal function, histology, EMT, and proteins related to the transforming growth factor-β (TGF-β)/Smad signaling pathway in the remnant kidneys were examined 8 weeks after surgery, compared with non-cell patch controls.
**RESULTS:** The DKSs were acellular and porous, with rich cytokine and major extracellular matrix components. The ucMSCs were distributed uniformly in the DKSs. Renal function was improved, renal fibrosis and EMT were reduced, and the TGF-β/Smad signaling pathway was inhibited compared with controls at 8 weeks after ucMSC-DKS patch transplantation.
**CONCLUSIONS:** The ucMSC-DKS restores renal function and reduces fibrosis by reducing EMT via the TGF-β/Smad signaling pathway in rats that have undergone STN. It provides an alternative for renal fibrosis treatment.

*Pediatric Research* (2020) 88:192–201; https://doi.org/10.1038/s41390-019-0736-6

## INTRODUCTION

Chronic kidney disease (CKD) is a public health problem worldwide, threatening individuals' health and burdening the social economy.[1,2] The main pathological changes in CKD include hypertrophy and loss of nephrons, dysfunction of glomerular filtration, and renal fibrosis.[3] Renal fibrosis is an essential mechanism by which CKD occurs and progresses, through inflammatory cell infiltration, the proliferation of fibroblasts, renal tubular dilation and atrophy, and extracellular matrix (ECM) deposition.[4] When the kidney is damaged, various inflammatory factors drive renal intrinsic cells, such as renal tubular epithelial cells, to transform into myofibroblasts, a process referred to as epithelial–mesenchymal transformation (EMT), and then to over-produce ECM, which accumulates in the renal interstitium.[5,6] EMT thus facilitates the development of renal fibrosis, and EMT inhibition reduces renal fibrosis and protects renal function.[7,8]

A large body of research has demonstrated that mesenchymal stem cells (MSCs) can contribute to the reduction of renal fibrosis by regulating several pathways, such as those of transforming growth factor-β (TGF-β)/Smad,[9] extracellular signal-related kinase 1/2,[10] and signal transducer and activator of transcription 3.[11] We have also shown previously that human umbilical cord MSCs (ucMSCs) alleviate inflammation and inhibit EMT, thereby reducing ECM deposition in renal fibrosis.[12,13] However, as most cellular transplantation is currently accomplished via intravascular injection, the maintenance of cell localization in the target organ is difficult. With the continuous development of tissue engineering, stem cells and three-dimensional scaffolds can be compounded for therapeutic use and tissue repair.[14] To contribute to efforts to keep cells in specific tissues so that they better perform their functions, we cultured ucMSC-loaded decellularized kidney scaffolds (DKSs) as cell patches, explored their effects on renal fibrosis, and elucidated the mechanism underlying these effects.

## MATERIALS AND METHODS

### Ethical considerations

This study, which involved humans and animals, was conducted according to the principles of the Declaration of Helsinki and was

[1]Department of Urology, Children's Hospital of Chongqing Medical University, 400014 Chongqing, China; [2]Chongqing Key Laboratory of Children Urogenital Development and Tissue Engineering, Chongqing Key Laboratory of Pediatrics, Ministry of Education Key Laboratory of Child Development and Disorders, National Clinical Research Center for Child Health and Disorders, China International Science and Technology Cooperation base of Child development and Critical Disorders, Children's Hospital of Chongqing Medical University, 400014 Chongqing, China; [3]Department of Pediatric Surgery, Chengdu Women's and Children's Central Hospital, School of Medicine, University of Electronic Science and Technology of China, 611731 Chengdu, China; [4]Department of Radiology, The Sixth Affiliated Hospital of Sun Yat-sen University, 510655 Guangzhou, China; [5]Biomanufacturing Center, Department of Mechanical Engineering, Tsinghua University, 100084 Beijing, China; [6]Institute for Regenerative Medicine, Sechenov University, 8-2 Trubetskaya Street, 119991 Moscow, Russia; [7]Research Institute for Uronephrology, Sechenov First Moscow State Medical University, 119991 Moscow, Russia and [8]Wake Forest Institute for Regenerative Medicine, Wake Forest School of Medicine, Winston-Salem, NC 27101, USA
Correspondence: Deying Zhang (zdy@hospital.cqmu.edu.cn) or Guanghui Wei (u806806@cqmu.deu.cn)

Received: 30 April 2019 Revised: 28 September 2019 Accepted: 2 October 2019
Published online: 2 January 2020

approved by the ethics committee of Chongqing Medical University. Male Sprague–Dawley (SD) rats weighing 180–220 g were provided by and raised at Chongqing Medical University (specific pathogen free, license no. SYXK [Chongqing] 2017-0001). All rats were maintained in polycarbonate cages under a 12/12-h light/dark cycle with free access to water and food.

### DKS preparation

Thirty rats were anesthetized with 20 mg/ml avertin (Sigma, St. Louis, MO), and the left kidneys were obtained by aseptic operation with preservation of the renal artery, renal vein, and ureter. The specimens were placed in cold (4 °C) sterilized phosphate-buffered saline (PBS). A 26-gauge intravenous cannula needle (Puyi, Shanghai, China) was immediately inserted into the renal artery, ligated with silk suture, and connected to a peristaltic tubing pump (Chuangrui, Hebei, China) to allow continuous rinsing with various solutions. Cold (4 °C) sterilized PBS containing 50 U/ml heparin sodium (Qianhong, Jiangsu, China) was then perfused through the artery at a rate of 4 ml/min to prevent the formation of thrombosis. The isolated kidneys were frozen at −80 °C for 3 h and then thawed at 4 °C for 6 h; three freeze-thawing cycles were then performed, with perfusion of cold (4 °C) 0.1% Triton X-100 (10 ml/min; Solarbio, Beijing, China) for 3 h and 0.5% sodium dodecyl sulfate (SDS, 10 ml/min; Solarbio) for 20 min. The resulting DKSs were rinsed with cold (4 °C) sterilized PBS with 100 U/ml penicillin G and 100 U/ml streptomycin for 24 h (4 ml/min) to remove residual perfused materials.

### Procurement and culture of human ucMSCs

Human ucMSCs were provided by the Stem Cell Center of the Children's Hospital of Chongqing Medical University, and we have previously described their procurement and characteristics.[12,15] The cells were cultured in Dulbecco's modified Eagle's medium/nutrient mixture F-12 Ham (DMEM/F-12; Sigma) with 1% penicillin/streptomycin (Gibco, Grand Island, NY) and 10% fetal bovine serum (FBS; Gibco, Grand Island, NY) at 37 °C with 5% $CO_2$. The culture medium was replaced every 3 days.

### Recellularization of DKSs with ucMSCs

To achieve even seeding of ucMSCs in the DKSs, we conducted a series of experiments in which the cells were delivered via different vascular pathways. First, the entire DKS was suspended in the vacuum chamber of a sterile three-port glass bottle under −50 mmHg pressure created by a vacuum pump (Yuwell, Jiangsu, China). Unicellular culture medium suspensions (1 ml) containing $5 \times 10^7$ ucMSCs were perfused into the DKS via the arterial cannula at a rate of 1 ml/min. The culture medium was sequentially perfused at a higher flow rate of 10 ml/min for 1 min to facilitate cell delivery. Then, 60–80 ml medium was poured into the chamber, cyclically perfused into the scaffold, and immersed and suspended in the medium. The system was incubated at 37 °C with 5% $CO_2$. To provide the appropriate gas conditions, 5% $CO_2$ was pumped continuously into the medium from the incubator. After 6 h, the scaffold was continuously perfused with culture medium at a rate of 1 ml/min. During the 5-day culture period, the medium was changed every 48 h.

In a second series of experiments, after cannulation of the preserved ureters, $5 \times 10^7$ ucMSCs were perfused through each ureter cannula at the same two sequential flow rates, and in the same vacuum environment. The scaffold recellularized through the ureter was cultured continuously in vitro for 5 days under the same conditions.

In the last series of experiments, the first and second cell seeding procedures were combined. In brief, $2.5 \times 10^7$ ucMSCs were delivered through the renal artery 12 h after $2.5 \times 10^7$ cells had been delivered through the ureter. The scaffold was cultured in vitro under the same conditions.

### Surgical procedure

The SD rats were divided randomly into four groups ($n = 6$/group) that underwent sham surgical incision (sham group), subtotal (5/6) nephrectomy (STN group), STN and DKS transplantation (DKS group), and STN and ucMSC-loaded DKS transplantation (ucMSC-DKS group), respectively. The surgery was performed as shown in Fig. 1. After the induction of anesthesia (20 mg/ml avertin; Sigma), the right kidney was exposed in compliance with asepsis through a small left flank incision. The adrenal gland and perirenal fat were separated from the right kidney, followed by ligation of the renal artery, renal vein, and ureter with 4-0 silk. The right kidney was then removed, and the abdominal incision was sutured in layers. Seven days later, the left kidney was dissociated in the same way. The upper and lower thirds of the left kidney were resected after blood occlusion. The remaining kidney thirds in rats in the STN group were sutured directly after pressing with gauze; those in the DKS and ucMSC-DKS groups were sutured with half of similarly sized DKSs and ucMSC-DKSs ($8 \times 8$ mm$^2$), respectively. Care was taken to ensure that the cut ends of the remnant kidneys and the patches were sutured superficially; the renal capsule was used when necessary. After 30 min blood occlusion, the ligation was removed to restore perfusion. In the absence of obvious bleeding, the abdominal incision was then sutured. Abdominal incision and kidney dissociation only were performed in the sham group. Rats in all groups were euthanized in the 8th week after the second operation for collection of the remnant kidneys and blood. Biochemical analysis, including serum creatinine (SCr) and blood urea nitrogen (BUN) measurement, was conducted.

### Histological examination

The kidneys, DKSs, and ucMSC-DKSs were fixed with 4% paraformaldehyde, dehydrated with alcohol and xylene, embedded in paraffin, and cut into 4-μm slices. After dewaxing with xylene and hydration in a graded series of alcohol concentrations, the slices were stained with hematoxylin and eosin (HE), diamidino-phenyl-indole (DAPI), periodic acid-Schiff (PAS) and Masson's trichrome, according to established protocols.

### Immunofluorescence

Antigens were retrieved by microwave heating of the dewaxed, hydrated kidney, and scaffold slices in citric acid buffer (pH 6.0) and endogenous peroxidase blocked in 3% $H_2O_2$. The slices were treated for 1 h with 0.5% bovine serum to block nonspecific protein binding sites, and then incubated at 4 °C overnight with 1:200 diluted mouse anti-collagen I antibody (Santa Cruz Biotechnology, Santa Cruz, CA), rabbit anti-collagen III antibody (Boster, Wuhan, China), mouse anti-collagen IV antibody (Santa Cruz Biotechnology), mouse anti-fibronectin antibody (Santa Cruz Biotechnology), mouse anti-laminin antibody (Santa Cruz Biotechnology), mouse anti-proliferating cell nuclear antigen (PCNA) antibody (Santa Cruz Biotechnology), and mouse anti-E-cadherin antibody (Cell Signaling Technology, Danvers, MA) mixed with rabbit anti-α-smooth muscle actin (α-SMA) antibody (Abcam, Cambridge, MA). On the next day, fluorescent secondary antibodies (ZSGB-BIO, Beijing, China) were applied and the samples were incubated at room temperature for 1 h. The specimens were counterstained with DAPI and examined under a fluorescence microscope (Nikon, Tokyo, Japan).

### Flow distribution assay

To determine the distribution of culture medium flowing in and spilling out of the vasculature in DKSs during perfusion, the medium was perfused at 1 ml/min from the renal artery. The volume of fluid exiting through the renal vein and from the outer surfaces was measured for a 0.5-h period.

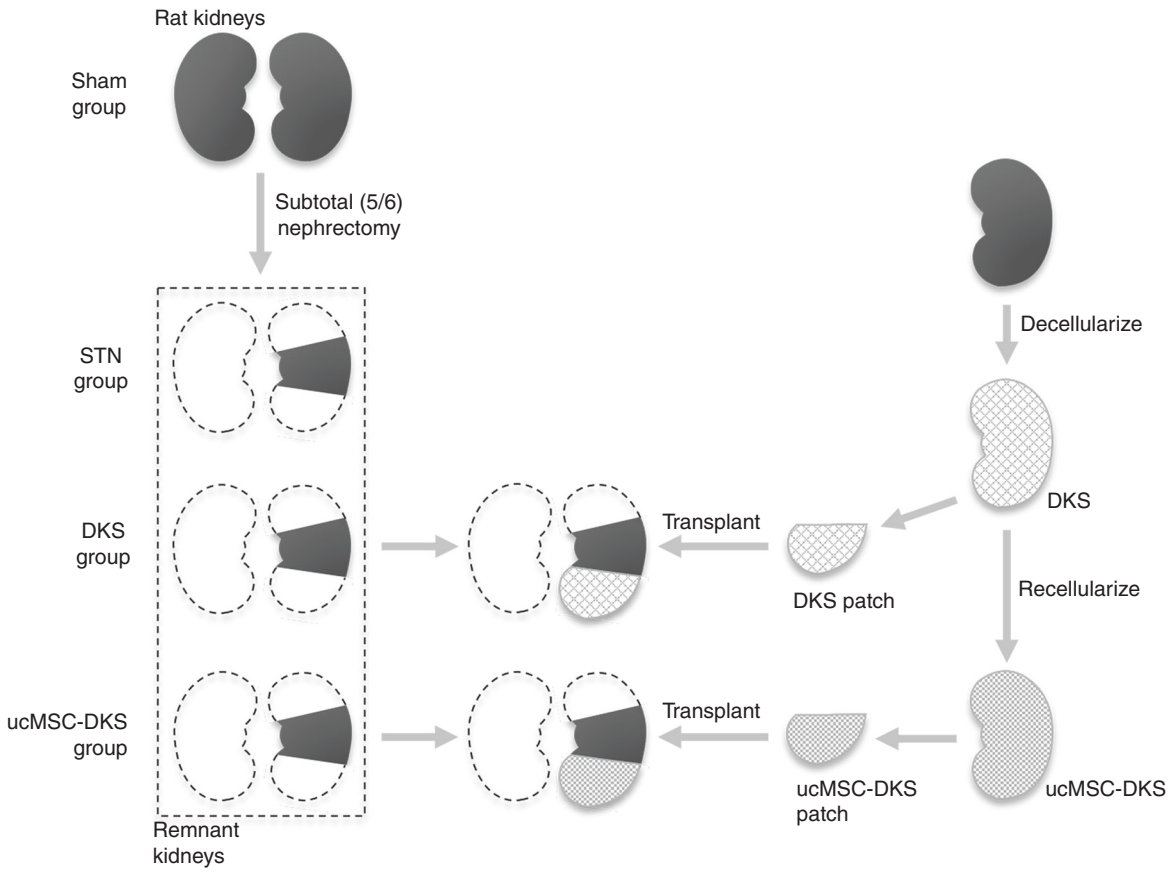


**Fig. 1 Experimental grouping and surgical procedure.** Subtotal (5/6) nephrectomy (STN) and transplantation of decellularized and umbilical cord mesenchymal stem cell-loaded decellularized kidney scaffold patches (ucMSC-DKSs).

DNA quantification

The native kidneys and freshly prepared DKSs were freeze dried for 12 h using a freeze dryer (Thermo, Waltham, MA) to ascertain dry weights. The E.Z.N.A.® Tissue DNA Kit (Omega Bio-Tek, Gaithersburg, MD) was used to extract DNA, according to the manufacturer's instructions. DNA concentrations were quantified by spectrophotometry (Thermo).

Scanning electron microscopy

The DKSs were washed in normal saline, fixed with glutaraldehyde and osmium tetroxide, dehydrated, and gold coated. They were then observed under a scanning electron microscope (Hitachi, Tokyo, Japan).

In vitro DKS cytotoxicity assay

The biological evaluation of DKSs was carried out according to ISO 10993-5: 1999. Briefly, irrigated and non-irrigated DKSs were immersed in warm (37 °C) FBS-free DMEM/F-12 at the rate of 1 mg/ml for 24 h; 10% FBS was then added for extract preparation. Human ucMSCs were plated into 96-well plates at a density of $5.0 \times 10^3$ cells per well and cultured for 24 h. The cells were then incubated with DMEM/F-12 containing 10% FBS, with or without 0.1% Triton X-100 or 0.5% SDS, or extracts for 6, 12, 24, and 48 h. After exposure, 20 µl 5-mg/ml 3-(4,5)-dimethylthiahiazo(-z-y1)-3,5-di-phenytetrazoliumromide (Solarbio) was added to the wells. After incubation at 37 °C for 4 h, the cells were treated with 100 µl dimethyl sulfoxide. Absorbance at 492 nm was quantified by spectrophotometry (Omega Bio-Tek).

Growth factor quantification assays

The lyophilized native kidneys and DKSs were dissolved in 1 ml radioimmunoprecipitation assay lysis buffer (Beyotime, Shanghai, China) with 1 mmol/l phenyl methyl sulfonyl fluoride (Beyotime), with the involvement of a tissue tearor. The lysates were sonicated for 10 min, and then centrifuged at $13{,}000 \times g$ for 10 min. The concentrations of various cytokines, including vascular endothelial growth factor (VEGF), epidermal growth factor (EGF), insulin-like growth factor-1 (IGF-1), and platelet-derived growth factor-BB (PDGF-BB), in the supernatants were determined with the rat VEGF (Neobioscience, Shenzhen, China), rat EGF (Neobioscience), rat bFGF (Neobioscience), rat IGF-1 (Elabscience, Wuhan, China), and rat PDGF-BB (Elabscience) enzyme-linked immunosorbent assay (ELISA) kits, respectively.

Western blot analysis

The protein concentrations in lysed and centrifuged remnant kidneys were measured using a bicinchoninic acid assay kit (Beyotime). The protein samples were mixed with SDS-polyacrylamide gel electrophoresis (SDS-PAGE) loading buffer, and then boiled for 10 min. They were electrophoresed through SDS-PAGE gel, and then transferred to polyvinylidene fluoride membranes (Merck Millipore, Billerica, MA). The membranes were incubated for 1 h in 5% skim milk on a shaker to block nonspecific protein binding. Primary antibodies against rabbit anti-TGF-β1 (1:1000; Abcam), rabbit anti-phospho-Smad 2/3 (p-Smad 2/3, 1:1000; Cell Signaling Technology), rabbit anti-Smad 7 (1:1000; Abcam), mouse anti-E-cadherin (1:1000; Cell Signaling Technology), rabbit anti-α-SMA (1:1000; Abcam), and mouse anti-β-actin (1:500; ZSGB-BIO) were incubated with the membranes at 4 °C overnight. The membranes were washed three times with Tris-buffered saline/Tween, and then incubated for 1 h with corresponding secondary antibodies (ZSGB-BIO). The ChemiDoc™ Touch Imaging System (Bio-Rad Laboratories, Hercules, CA) was used for band detection, and

positive immune reactions were analyzed using the Image J software.

### Statistical analysis

Quantitative experimental data were reported as means ± standard deviations. The independent-samples *t* test (for two groups) and one-way analysis of variance (for multiple groups) were used for comparison. The analyses were performed using SPSS 18.0 (SPSS Inc., Chicago, IL) with a significance level of 0.05.

## RESULTS

### NDKS characteristics

During the whole decellularization process, the color of the native kidneys became lighter after repeated freeze thawing, then white, and gradually transparent from the cortex to the medulla after sequential perfusion with Triton X-100 and SDS solutions (Fig. 2a). Eosinophilic HE staining of the ECM, including intact glomerular and tubular basement membranes, but no basophilic nuclear staining, was observed (Fig. 2b). Similarly, DAPI staining revealed no blue nuclear fluorescence (Fig. 2c). The DNA content of DKSs was reduced from 12,414.75 ± 699.29 ng/mg to 40.18 ± 5.71 ng/mg (Fig. 2d), which meets the biocompatibility standard for acellular ECM in tissue engineering.[16] Masson's trichrome staining confirmed the preservation and integrity of collagen in the ECM of the DKSs (Fig. 2e). The corresponding characteristic PAS polysaccharide staining was also observed (Fig. 2f). Scanning electron microscopy showed that the ECM of DKSs retained the original globular and tubular stereostructures (Fig. 2g). Immunofluorescence confirmed the expression of major structural proteins, including collagen I, collagen III, collagen IV, fibronectin, and laminin, which constitute the ECM in DKSs (Fig. 2h). To enable better DKS recellularization by perfusion, the distribution of fluid in the DKSs was assessed to determine the fluid flow path. Compared with that in native kidneys, a significantly larger proportion of fluid spilled from the outer walls of the DKSs ($p < 0.01$), reflecting the perviousness of the DKSs (Fig. 2i). ELISA quantification showed the retention to some extent of VEGF, EGF, IGF-1, and PDGF-BB in the DKSs (Fig. 2j). The in vitro cytotoxicity assay confirmed that the flushed DKS extracts had no obvious cytotoxicity, suggesting the innocuousness of the scaffolds as supporting structures for cell growth (Fig. 2k).

### ucMSC-loaded DKS characteristics

HE staining revealed that the perfusion of human ucMSCs through the renal artery alone resulted in abundant cell distribution in the glomerular region, but sparse and scattered distribution in the renal tubule region (Fig. 3a). The perfusion of cells through the ureter alone resulted in the distribution of abundant cells in the tubular regions of the DKSs and the formation of tubule-like hollow structures, but few cells in the glomerular region. Sequential cell perfusion through the renal artery and ureter resulted in abundant cell distribution in the glomerular and tubular regions of the DKSs, with the formation of tubule-like structures. Immunofluorescence staining showed that some ucMSCs cultured in DKSs expressed PCNA, indicating active cell proliferation (Fig. 3b).

### Renal pathology and function after transplantation of human ucMSCs cultured in DKSs

Gross morphological changes in the kidneys at 8 weeks after surgery are shown in Fig. 4a. Kidneys in the sham group were smooth, tender, and ruddy. Those in the STN and DKS groups were reddish-yellow and exhibited surface graininess, with scarring on the upper and lower sections. Kidneys in the ucMSC-DKS group were also reddish-yellow, but without obvious granules. The different degrees of kidney damage are shown by HE staining in Fig. 4b. Kidneys in the sham group showed clear glomerular and tubular structures, without obvious inflammatory cell infiltration, whereas those in the STN and DKS groups showed some fibrous glomerulus and atrophic tubules, with fibrous proliferation and inflammatory cell infiltration. Compared with the STN group, the ucMSC-DKS group showed less glomerular fibrosis, tubular atrophy, and inflammatory cell infiltration. Collagenous fibers accumulated in the ECM showed weak blue staining by Masson's trichrome in the sham group, and thick bedding and disorder in the STN and DKS groups. Fewer fibers were observed in the ucMSC-DKS group than in the STN group (Fig. 4c). SCr and BUN levels in the STN group were significantly higher than those in the sham group (both $p < 0.01$), but similar to those in the DKS group. SCr and BUN levels were significantly decreased after ucMSC-DKS patch transplantation (SCr, $p < 0.05$; BUN, $p < 0.01$; Fig. 4d).

### EMT and TGF-β/Smad signaling pathway expression after ucMSC-DKS patch transplantation

Immunofluorescence staining showed increased co-expression of E-cadherin (a renal tubular epithelial marker) and α-SMA (a fibroblast marker), indicating ongoing EMT, in the STN group compared with the sham group, and decreased co-expression in the ucMSC-DKS group compared with the STN group (Fig. 5a). Western blotting also showed lesser E-cadherin expression and greater α-SMA expression in the STN group compared with the sham group, and inverse variation of these expression levels in the ucMSC-DKS group compared with the STN group. The DKS patch alone did not affect E-cadherin or α-SMA expression (Fig. 5b). These results suggest that the ucMSCs inhibited EMT in renal fibrosis.

Western blot analysis indicated that the expression levels of TGF-β1 and p-Smad 2/3 were increased in the STN group compared with the sham group, and decreased in the ucMSC-DKS group compared with the STN group (both $p < 0.05$; Fig. 5c). The expression of Smad 7 correlated inversely with that of TGF-β1. TGF-β1, p-Smad 2/3, and Smad 7 expression was similar in the STN and DKS groups. These results suggested that the ucMSCs inhibited TGF-β/Smad signaling pathway activation in rats that had undergone STN.

## DISCUSSION

Feasible kidney-tissue engineering strategies require appropriate cell populations, efficient scaffolds, and three-dimensional culture conditions.[17] Given their good biocompatibility, low immunogenicity, and adequate vasculature, which provides a dynamic environment for cells,[18,19] DKSs were prepared in this study by freeze thawing with detergent to establish niches for cell growth and proliferation. Repeated freezing and thawing contributed to cellular removal through the formation of ice crystals in the cells and the destruction of cell membranes.[20] Triton X-100 and SDS at low concentrations were then used to decellularize the kidneys in less time than achieved in other studies,[21–23] with the greatest retention of ECM content, physiological activity, and spatial structure. The characterization of DKSs confirmed the retention of major ECM components, other than renal cells, and the porous, non-cytotoxic, and cytokine-rich nature of the DKSs, suggesting that the scaffolds can support the growth and proliferation of cells. In addition, the examination of flow distribution revealed the permeability of the DKSs, with niches for cells available in the attachment surfaces. Our analyses also suggested that the recellularization of all DKS vasculature, to the greatest extent possible, is necessary to avoid plasma spillage after transplantation.

Previous studies have suggested that human ucMSCs attenuate inflammation, oxidative stress, and fibrosis progression in acute kidney injury.[24,25] In view of their protective role, we used ucMSCs

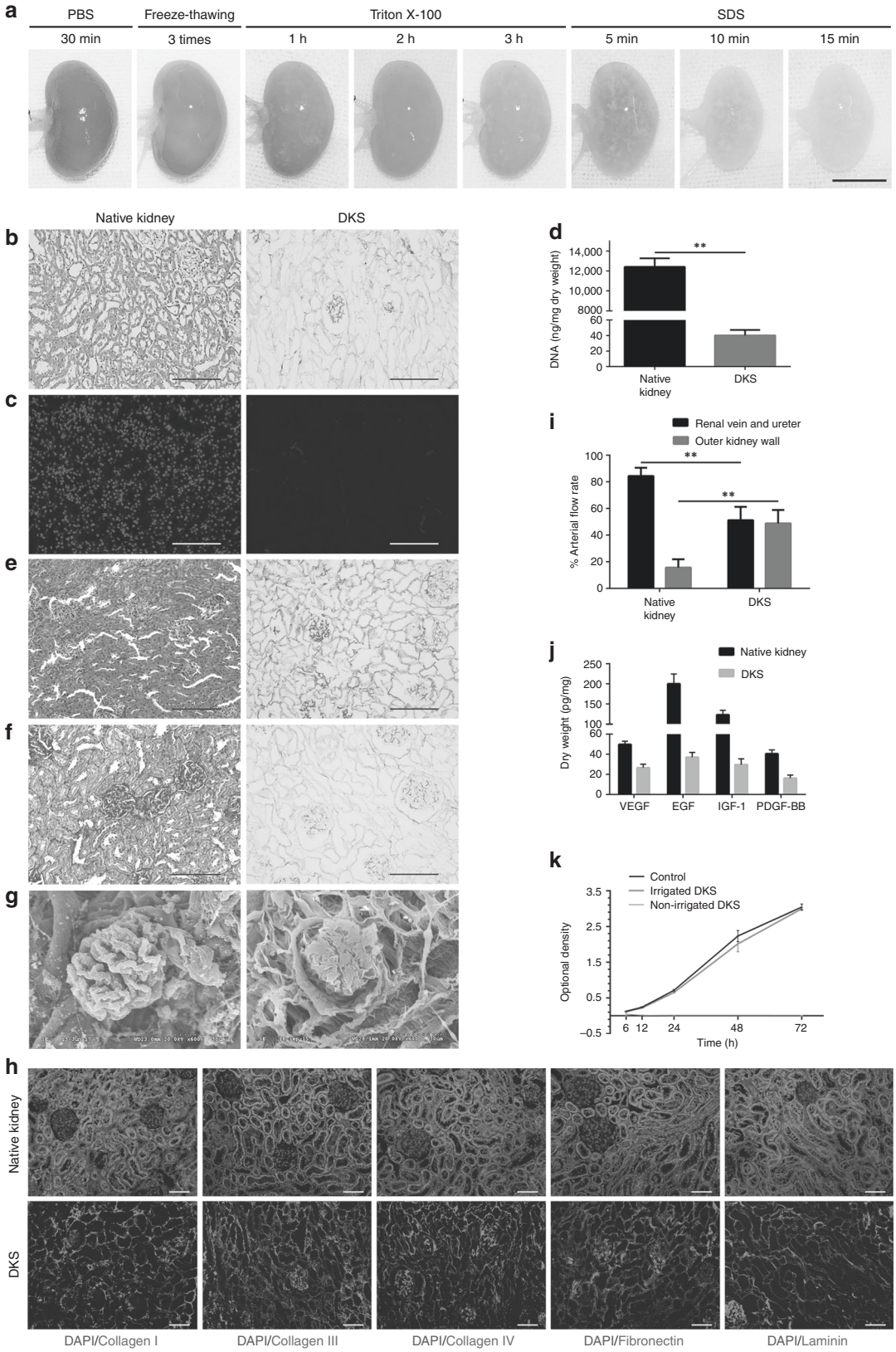


**Fig. 2 Characterization of decellularized kidney scaffolds (DKSs). a** Gross morphological changes during decellularization in each group (bar, 1 cm). Hematoxylin–eosin staining (**b**; bar, 100 μm), diamidino-phenyl-indole (DAPI) staining (**c**; bar, 100 μm), DNA quantification (**d**), Masson's trichrome staining (**e**; bar, 100 μm), periodic acid-Schiff staining (**f**; bar, 100 μm), and scanning electron microscopy (**g**; bar, 30 μm) of native kidneys and DKSs. **h** Immunofluorescence staining for the main structural protein in the extracellular matrix of native kidneys and DKSs (bar, 100 μm). **i** Flow distribution in native kidneys and DKSs (**$p < 0.01$). Growth factor quantification (**j**) and in vitro cytotoxicity assay (**k**) for native kidneys and DKSs. PBS, phosphate-buffered saline; SDS, sodium dodecyl sulfate; VEGF, vascular endothelial growth factor; EGF, epidermal growth factor; IGF-1, insulin-like growth factor-1; PDGF-BB, platelet-derived growth factor-BB.

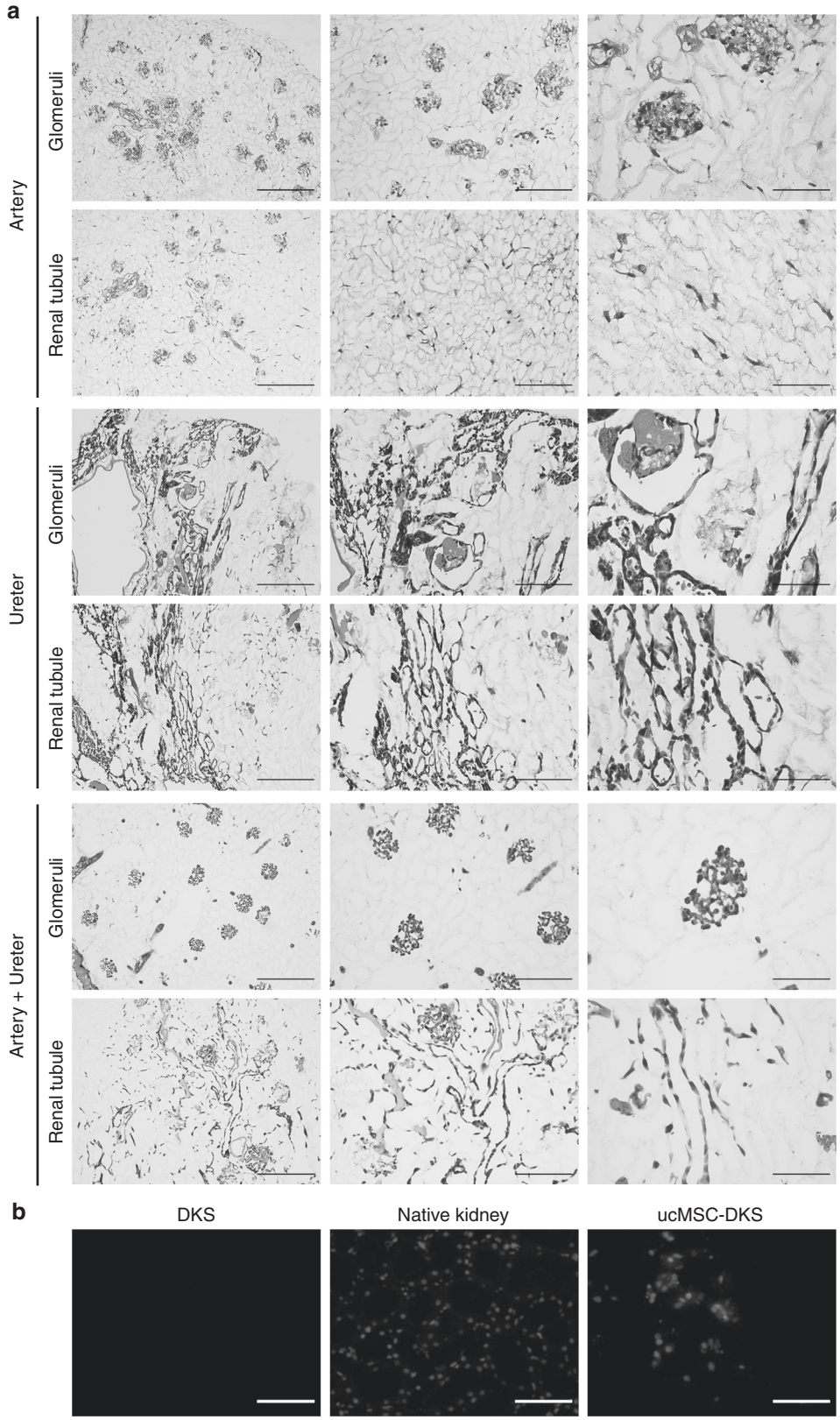


**Fig. 3 Characterization of umbilical cord mesenchymal stem cell-loaded decellularized kidney scaffolds (ucMSC-DKSs).** **a** Hematoxylin–eosin staining for cell distribution in ucMSC-DKSs (bars: left, 200 μm; middle, 100 μm; right, 50 μm). **b** Immunofluorescence staining for proliferating cell nuclear antigen in ucMSC-DKSs (bar, 100 μm).

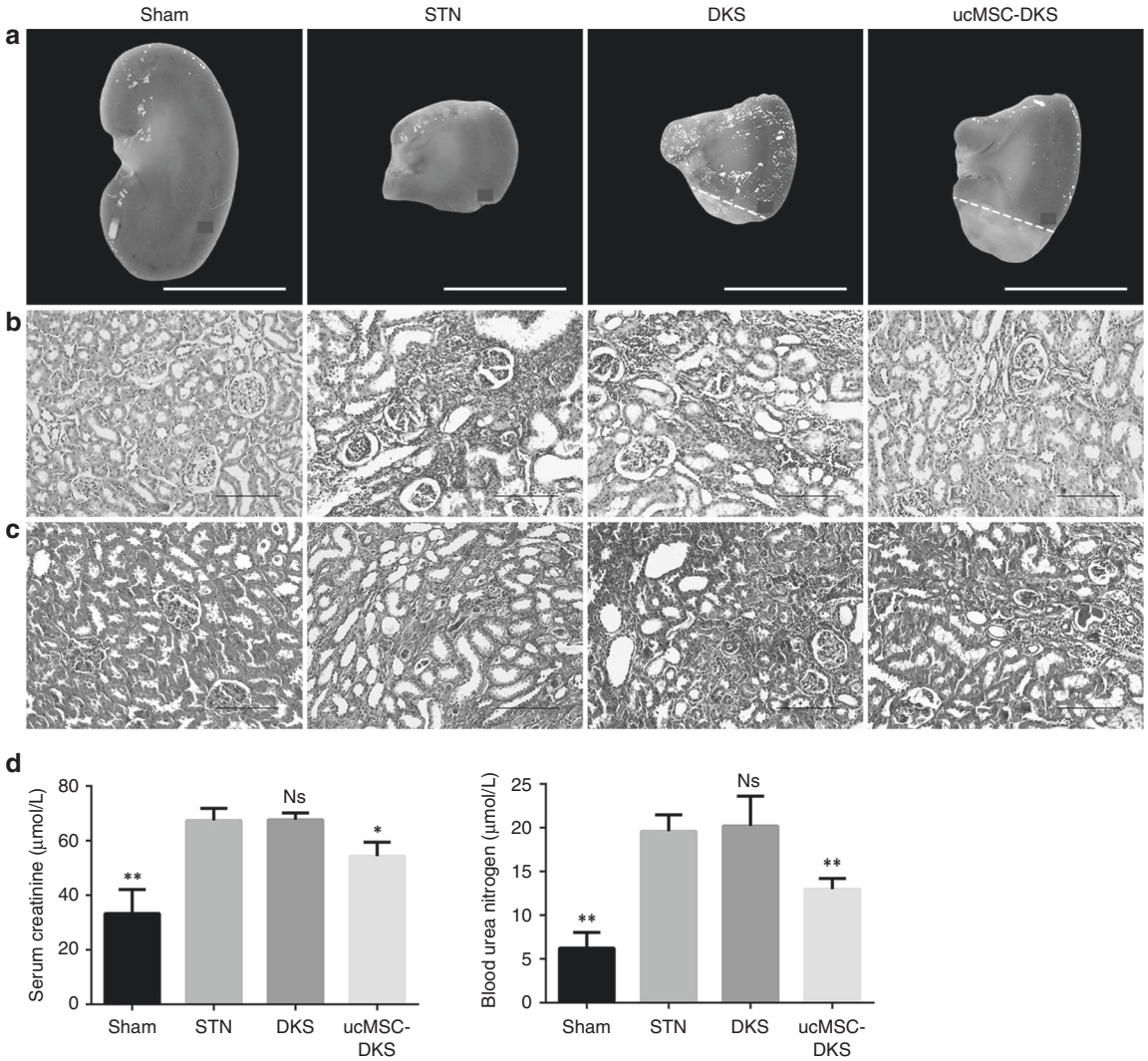


**Fig. 4 Renal pathology and function after umbilical cord mesenchymal stem cell-loaded decellularized kidney scaffold (ucMSC-DKS) patch transplantation. a** Gross morphological changes in kidneys in each group (bar, 1 cm). Hematoxylin–eosin (**b**) and Masson's trichrome (**c**) staining of remnant kidneys in each group (bars, 100 μm). **d** Serum creatinine and blood urea nitrogen levels in each group (*$p < 0.05$, **$p < 0.01$). STN, subtotal (5/6) nephrectomy. NS, not significant.

to seed the DKSs and thereby rebuild cell-scaffold compounds. Whole-DKS seeding has typically been performed by the perfusion of cell suspensions through the renal artery or ureter; the pathway of cell delivery to DKSs is critical because of differences among extracellular compartments in the effects of ECM-mediated cell signaling. With consideration of the kidney's disconnected vascular system and its collecting system, we adopted perfusion pathways through the artery and ureter to achieve uniform cell redistribution. The results showed abundant cell distribution in the vascular and collecting systems; in particular, cells in the tubular regions attached to the ECM, forming hollow tubule-like structures. We inferred that these tubular-like structures could reduce plasma spillage when a recellularized scaffold is transplanted into a kidney. Moreover, our findings reveal the potential for kidney regeneration. The observed PCNA expression further demonstrated that the DKSs provided niches for ucMSC proliferation in vitro. Thus, we successfully constructed a human ucMSC-rich DKS complex that may contribute to protection against kidney injury.

We prepared an established rat model of renal fibrosis[26,27] and demonstrated the impairment of renal function along with glomerulosclerosis, inflammatory cell infiltration, and interstitial fibrosis. We observed increased expression of α-SMA, marking myofibroblasts, and decreased expression of E-cadherin in renal tubular epithelial cells, used to detect the occurrence of EMT, in this model. The immunofluorescence and western blot analyses showed that the ucMSC-DKS patch reduced EMT in rats that had undergone STN, whereas the DKS alone had no significant effect. Studies have confirmed that the EMT of renal tubular epithelial cells is associated with TGF-β/Smad,[28] Wnt/β-catenin,[29] and Notch[30] signaling pathways. TGF-β1, an initial molecule regulating the synthesis and degradation of ECM proteins, can bind to and recruit the membrane-bound TGF-β1 receptor (TβR) and activate receptor-regulated Smads (R-Smads; e.g., Smad 2 and Smad 3). Thereafter, R-Smad bound to Smad 4 enters the nucleus and regulates target gene transcription.[31,32] Smad 7, an inhibitory Smad, can bind to the TβR and inhibit the activation of Smad signaling.[33] In our study, the expression of TGF-β1 and p-Smad 2/3 was decreased after ucMSC-DKS transplantation, whereas that of Smad 7 was increased. DKS transplantation alone had no effect on the expression of TGF-β1, p-Smad 2/3, or Smad 7. Thus, we infer that the ucMSCs seeded

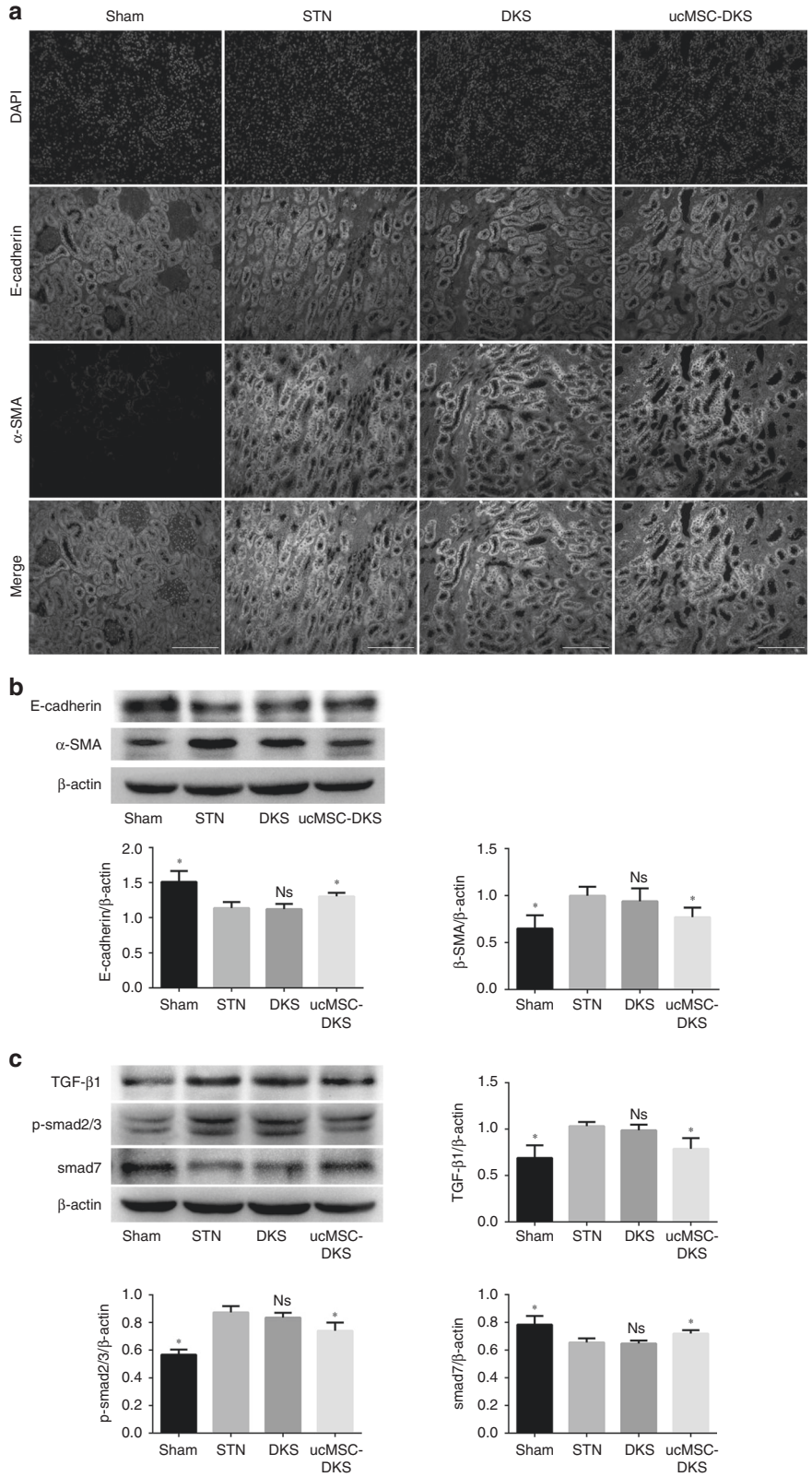


**Fig. 5 Epithelial–mesenchymal transition and transforming growth factor-β1 (TGF-β1)/Smad signaling pathway expression after umbilical cord mesenchymal stem cell-loaded decellularized kidney scaffold (ucMSC-DKS) patch transplantation. a** Co-immunofluorescence staining of remnant kidneys for E-cadherin and α-smooth muscle actin (α-SMA) in each group (bar, 100 μm). **b** Western blot analysis of E-cadherin and α-SMA expression in remnant kidneys in each group [$^{*}p < 0.05$ vs. sham group, $^{\#}p < 0.05$ vs. subtotal nephrectomy (STN) group]. **c** Western blot analysis of TGF-β1, p-Smad 2/3, and Smad 7 expression in remnant kidneys in each group ($^{*}p < 0.05$ vs. sham group, $^{\#}p < 0.05$ vs. STN group). DAPI, diamidino-phenyl-indole. NS, not significant.

in the DKSs inhibited the TGF-β/Smad signaling pathway, playing a key role in the attenuation of renal fibrosis.

The pathophysiological process of renal fibrosis can be divided into four stages: (1) cell activation and injury, (2) fibrogenesis signaling stimulation, (3) fibrogenesis, and (4) destruction and progression.[34] We previously demonstrated that ucMSCs reduced renal fibrosis by reducing inflammation via toll-like receptor 4/nuclear factor-κB signaling in the first stage of pathophysiological changes. Based on this anti-inflammatory activity of ucMSCs, we focused on the TGF-β/Smad signaling pathway and its regulation of EMT in the second stage of pathophysiological changes in this study. Although our results suggest that ucMSCs cultured in DKSs attenuate renal fibrosis in rats that have undergone STN by reducing EMT via the TGF-β/Smad signaling pathway, the specific route of this effect is not clear; further research is required. Rats that have undergone STN exhibit oxidative stress, glomerular hypertension, and hyperfiltration.[35] These changes lead to persistent cell injury and the infiltration of inflammatory cells (e.g., B and T lymphocytes), which then secrete various inflammatory factors.[36] In the inflammatory environment, ucMSCs can secrete anti-inflammatory factors, which inhibit neutrophil and macrophage chemotaxis and dendritic cell maturation, and reduce B and T lymphocyte proliferation.[37] MSC-derived exosomes have also been reported to participate in the reduction of myocardial ischemia–reperfusion injury,[38] acute lung injury,[39] and acute kidney injury.[40] We speculate that ucMSCs seeded in DKSs ameliorate the inflammatory microenvironment and inhibit the TGF-β/Smad signaling pathway by secreting exosomes and/or cytokines, or in another as-yet unknown way. This study showed that a compound ucMSC-DKS patch attenuated renal fibrosis by reducing TGF-β/Smad-induced EMT. These findings generate new ideas for the application of tissue-engineered compound cell-scaffold patches and broaden the perspective on the treatment of CKD.

## CONCLUSIONS

Our results showed that a ucMSC-DKS patch, as a novel cell carrier, attenuated STN-induced renal fibrosis by reducing EMT via the TGF-β/Smad signaling pathway. The use of such patches might help to improve the retention of perfused cells in target organs, and bring new perspectives on the treatment of CKD. Further studies are needed to determine the long-term effects of ucMSC-DKSs on the attenuation of renal fibrosis and inflammation, and on renal function recovery.

## FUNDING

This work was supported by grants from the National Natural Science Foundation of China (nos. 81800618, 81771566) and the Chongqing Research Program of Basic Research and Frontier Technology (no. cstc2018jcyjAX0193).

## AUTHOR CONTRIBUTIONS

Hu D, Zhang D, Liu B, Liu Y and Wei G contributed to the conception and design of the study and manuscript preparation. Hu D, Liu B, Liu Y, Shen L, Long C, Zhang D, Liu X, Lin T and He D were responsible for the cell experiments, data collection, and manuscript writing. Hu D, Zhang D, Zhou Y, Yu Y, Xu T, Timashev P, Butnaru D, Zhang Y and Wei G were involved in animal experiments, data collection, and manuscript editing. All authors read and approved the final version of the manuscript.

## ADDITIONAL INFORMATION

The online version of this article (https://doi.org/10.1038/s41390-019-0736-6) contains supplementary material, which is available to authorized users.

**Competing interests:** The authors declare no competing interests.



## REFERENCES

1. Zhang, L. et al. Prevalence of chronic kidney disease in China: a cross-sectional survey. *Lancet* **379**, 815–822 (2012).
2. Webster, A. C., Nagler, E. V., Morton, R. L. & Masson, P. Chronic kidney disease. *Lancet* **389**, 1238–1252 (2017).
3. Romagnani, P. et al. Chronic kidney disease. *Nat. Rev. Dis. Prim.* **3**, 17088 (2017).
4. Zeisberg, E. M., Potenta, S. E., Sugimoto, H., Zeisberg, M. & Kalluri, R. Fibroblasts in kidney fibrosis emerge via endothelial-to-mesenchymal transition. *J. Am. Soc. Nephrol.* **19**, 2282–2287 (2008).
5. Lovisa, S., Zeisberg, M. & Kalluri, R. Partial epithelial-to-mesenchymal transition and other new mechanisms of kidney fibrosis. *Trends Endocrinol. Metab.* **27**, 681–695 (2016).
6. Yin, J. et al. Apelin inhibited epithelial–mesenchymal transition of podocytes in diabetic mice through downregulating immunoproteasome subunits β5i. *Cell Death Dis.* **9**, 1031 (2018).
7. Sun, Z. et al. miR-133b and miR-199b knockdown attenuate TGF-β1-induced epithelial to mesenchymal transition and renal fibrosis by targeting SIRT1 in diabetic nephropathy. *Eur. J. Pharm.* **837**, 96–104 (2018).
8. Cai, P., Liu, X., Xu, Y., Qi, F. & Si, G. Shenqi detoxification granule combined with P311 inhibits epithelial–mesenchymal transition in renal fibrosis via TGF-β1-Smad-ILK pathway. *Biosci. Trends* **11**, 640–650 (2017).
9. Song, Y. et al. Adipose-derived stem cells ameliorate renal interstitial fibrosis through inhibition of EMT and inflammatory response via TGF-β1 signaling pathway. *Int. Immunopharmacol.* **44**, 115–122 (2017).
10. Chen, W., Yan, Y., Song, C., Ding, Y. & Du, T. Microvesicles derived from human Wharton's Jelly mesenchymal stem cells ameliorate ischemia–reperfusion-induced renal fibrosis by releasing from G2/M cell cycle arrest. *Biochem. J.* **474**, 4207–4218 (2017).
11. Matsui, F. et al. Mesenchymal stem cells protect against obstruction-induced renal fibrosis by decreasing STAT3 activation and STAT3-dependent MMP-9 production. *Am. J. Physiol. Ren. Physiol.* **312**, F25–F32 (2017).
12. Liu, B. et al. Human umbilical cord mesenchymal stem cell conditioned medium attenuates renal fibrosis by reducing inflammation and epithelial-to-mesenchymal transition via the TLR4/NF-κB signaling pathway in vivo and in vitro. *Stem Cell Res. Ther.* **9**, 7 (2018).
13. Liu, B. et al. Human umbilical cord-derived mesenchymal stem cells conditioned medium attenuate interstitial fibrosis and stimulate the repair of tubular epithelial cells in an irreversible model of unilateral ureteral obstruction. *Nephrology (Carlton)* **23**, 728–736 (2018).
14. Langer, R. & Vacanti, J. P. Tissue engineering. *Science* **260**, 920–926 (1993).
15. Li, D. et al. Exosomes from human umbilical cord mesenchymal stem cells reduce damage from oxidative stress and the epithelial–mesenchymal transition in renal epithelial cells exposed to oxalate and calcium oxalate monohydrate. *Stem Cells Int.* **2019**, 6935806 (2019).
16. Crapo, P. M., Gilbert, T. W. & Badylak, S. F. An overview of tissue and whole organ decellularization processes. *Biomaterials* **32**, 3233–3243 (2011).
17. Batchelder, C. A., Martinez, M. L. & Tarantal, A. F. Natural scaffolds for renal differentiation of human embryonic stem cells for kidney tissue engineering. *PLoS ONE* **10**, e0143849 (2015).
18. Poornejad, N. et al. Efficient decellularization of whole porcine kidneys improves reseeded cell behavior. *Biomed. Mater.* **11**, 025003 (2016).
19. Peloso, A. et al. Creation and implantation of acellular rat renal ECM-based scaffolds. *Organogenesis* **11**, 58–74 (2015).
20. Poornejad, N. et al. Freezing/thawing without cryoprotectant damages native but not decellularized porcine renal tissue. *Organogenesis* **11**, 30–45 (2015).
21. Chani, B., Puri, V., Sobti, R. C., Jha, V. & Puri, S. Decellularized scaffold of cryopreserved rat kidney retains its recellularization potential. *PLoS ONE* **12**, e0173040 (2017).
22. Sambi, M. et al. Acellular mouse kidney ECM can be used as a three-dimensional substrate to test the differentiation potential of embryonic stem cell derived renal progenitors. *Stem Cell Rev.* **13**, 513–531 (2017).
23. He, M., Callanan, A., Lagaras, K., Steele, J. & Stevens, M. M. Optimization of SDS exposure on preservation of ECM characteristics in whole organ decellularization of rat kidneys. *J. Biomed. Mater. Res. B* **105**, 1352–1360 (2017).
24. Rota, C. et al. Therapeutic potential of stromal cells of non-renal or renal origin in experimental chronic kidney disease. *Stem Cell Res. Ther.* **9**, 220 (2018).
25. Rodrigues, C. E. et al. Human umbilical cord-derived mesenchymal stromal cells protect against premature renal senescence resulting from oxidative stress in rats with acute kidney injury. *Stem Cell Res. Ther.* **8**, 19 (2017).
26. Yu, J. et al. MnTBAP therapy attenuates renal fibrosis in mice with 5/6 nephrectomy. *Oxid. Med. Cell Longev.* **2016**, 7496930 (2016).

27. Gong, W. et al. NLRP3 deletion protects against renal fibrosis and attenuates mitochondrial abnormality in mouse with 5/6 nephrectomy. *Am. J. Physiol. Ren. Physiol.* **310**, F1081–F1088 (2016).
28. Krafft, E. et al. Transforming growth factor beta 1 activation, storage, and signaling pathways in idiopathic pulmonary fibrosis in dogs. *J. Vet. Intern. Med.* **28**, 1666–1675 (2014).
29. Zhang, L. et al. C-reactive protein exacerbates epithelial–mesenchymal transition through Wnt/β-catenin and ERK signaling in streptozocin-induced diabetic nephropathy. *FASEB J.* https://doi.org/10.1096/fj201801865RR (2019).
30. Zhang, J. et al. Notch signaling modulates proliferative vitreoretinopathy via regulating retinal pigment epithelial-to-mesenchymal transition. *Histochem. Cell Biol.* **147**, 367–375 (2017).
31. Samarakoon, R. et al. Loss of expression of protein phosphatase magnesium-dependent 1A during kidney injury promotes fibrotic maladaptive repair. *FASEB J.* **30**, 3308–3320 (2016).
32. Loboda, A., Sobczak, M., Jozkowicz, A. & Dulak, J. TGF-β1/Smads and miR-21 in renal fibrosis and inflammation. *Mediat. Inflamm.* **2016**, 8319283 (2016).
33. Kavsak, P. et al. Smad7 binds to Smurf2 to form an E3 ubiquitin ligase that targets the TGF beta receptor for degradation. *Mol. Cell* **6**, 1365–1375 (2000).
34. Zambon, J. P. et al. Comparative analysis of two porcine kidney decellularization methods for maintenance of functional vascular architectures. *Acta Biomater.* **75**, 226–234 (2018).
35. Tapia, E. et al. Curcumin induces Nrf2 nuclear translocation and prevents glomerular hypertension, hyperfiltration, oxidant stress, and the decrease in antioxidant enzymes in 5/6 nephrectomized rats. *Oxid. Med. Cell Longev.* **2012**, 269039 (2012).
36. Mora-Fernández, C. et al. Diabetic kidney disease: from physiology to therapeutics. *J. Physiol.* **592**, 3997–4012 (2014).
37. Weil, B. R. et al. Mesenchymal stem cells attenuate myocardial functional depression and reduce systemic and myocardial inflammation during endotoxemia. *Surgery* **148**, 444–452 (2010).
38. Lai, R. C. et al. Exosome secreted by MSC reduces myocardial ischemia/reperfusion injury. *Stem Cell Res.* **4**, 214–222 (2010).
39. Zhu, Y. G. et al. Human mesenchymal stem cell microvesicles for treatment of *Escherichia coli* endotoxin-induced acute lung injury in mice. *Stem Cells* **32**, 116–125 (2014).
40. Bruno, S. et al. Microvesicles derived from mesenchymal stem cells enhance survival in a lethal model of acute kidney injury. *PLoS ONE* **7**, e33115 (2012).